magnetochemistry

MDPI

Article

Compatibility of $LaFe_{13-x-y}Mn_xSi_yH_{1.6}$ and Eutectic Liquid GaInSn Alloy †

Jamieson Brechtl [1,*], Joseph Rendall [1], Mingkan Zhang [1], Michael R. Koehler [2], Kashif Nawaz [1] and Ayyoub M. Momen [3]

[1] Buildings and Transportation Science Division, Oak Ridge National Laboratory, Oak Ridge, TN 37830, USA; rendalljd@ornl.gov (J.R.); zhangm1@ornl.gov (M.Z.); nawazk@ornl.gov (K.N.)
[2] IAMM Diffraction Facility, Institute for Advanced Materials & Manufacturing, University of Tennessee, Knoxville, TN 37920, USA; mkoehler@utk.edu
[3] Ultrasonic Technology Solutions, Knoxville, TN 37932, USA; ayyoubmomen@ultratechsol.com
* Correspondence: brechtljm@ornl.gov
† This manuscript has been authored in part by UT-Battelle, LLC, under contract DE-AC05-00OR22725 with the U.S. Department of Energy (DOE). The U.S. government retains the rights and the publisher, by accepting the article for publication, acknowledges that the U.S. government retains a nonexclusive, paid-up, irrevocable, worldwide license to publish or reproduce the published form of this manuscript, or allow others to do so, for U.S. government purposes. DOE will provide public access to these results of federally sponsored research in accordance with the DOE Public Access Plan (http://energy.gov/downloads/doe-public-access-plan, accessed on 12 November 2023).

Abstract: The heat transfer rate of magnetocaloric regenerators is a topic of extensive research and the cyclability of these regenerators is critical to the operation of systems with a high coefficient of performance (e.g., potentially >22, significantly higher than typical vapor compression cooling technologies). To enable a high operating frequency that will result in a high specific cooling power, the heat transfer fluid should have high thermal conductivity and lower specific heat, i.e., higher thermal diffusivity. Eutectic metal alloys possess these qualities, such as gallium–indium–tin (Galinstan), whose thermal diffusivity has been found to be approximately an order of magnitude higher than water. For this study, the effects of eutectic liquid Galinstan exposure on the phase stability of $LaFe_{13-x-y}Mn_xSi_yH_{1.6}$ magnetocaloric powders in an active magnetic regenerator device were investigated. The powders were characterized before and after exposure to Galinstan using X-ray diffraction, in which the phases were determined using the Rietveld refinement technique and X-ray fluorescence. It was found that after Galinstan exposure, hydrogen containing phases were present in the powder, suggesting that the hydrogen was lost from the magnetocaloric phase. The magnetocaloric phase degradation indicates that the powder was incompatible with the Galinstan metal in an environment with moisture.

Keywords: magnetocaloric powders; Galinstan; X-ray diffraction; magnetocaloric effect

Citation: Brechtl, J.; Rendall, J.; Zhang, M.; Koehler, M.R.; Nawaz, K.; Momen, A.M. Compatibility of $LaFe_{13-x-y}Mn_xSi_yH_{1.6}$ and Eutectic Liquid GaInSn Alloy. *Magnetochemistry* **2024**, *10*, 13. https://doi.org/10.3390/magnetochemistry10020013

Academic Editor: Paula Corte-Leon

Received: 13 November 2023
Revised: 7 January 2024
Accepted: 9 February 2024
Published: 12 February 2024

1. Introduction

Magnetocaloric materials (MCMs) are materials that exhibit a magnetocaloric effect (MCE), which is an adiabatic temperature or isothermal entropy change in response to a varying magnetic field [1]. Materials that have been explored in MCE studies include Gd and $Gd_5Ge_2Si_2$ [2,3], $LaFe_{11.74-y}Mn_ySi_{1.26}H_{1.53}$ (y = 0.32–0.39) [4], $LaFe_{11.2}Co_{0.7}Si_{1.1}$ [5], $La(Fe_{0.88}Si_{0.12})_{13}H_y$ (y = 0–1.6) [6], $MnAs_{1-x}Sb_x$ (x = 0.0–0.1) [7], and $MnFeP_{0.45}As_{0.55}$ [8] alloys. Of these materials, LaFeSi-based compounds have shown remarkable potential as a working material for room-temperature magnetic refrigeration due to factors including their high MCE, small hysteresis, and low cost [9]. One application of MCMs is in cooling processes such as active magnetic regenerative (AMR) refrigeration, as introduced by Barclay and Steyert [10], which uses a regenerative cycle to produce temperature spans that are comparable to conventional cooling systems [2].

Two recent reviews on active magnetic regenerators describe the physics of the MCM interaction with a magnetic field [11] and a summary of the coefficient of performance (COP) for AMR refrigerators ranging from 0.5 to 11.2—the latter being almost a 400% increase compared to typical refrigerators [12]. During an AMR cycle, the MCE is utilized by repeatedly raising and lowering the temperature of the MCM by changing the external magnetic field to create a heat-pumping effect [2,12]. The MCM is usually packed in a flow conduit called the regenerator (e.g., tube). Heat transfer fluid (HTF) is alternately pumped in both directions along the axis of the regenerator to add and remove heat to and from the MCM as it undergoes magnetization and demagnetization.

High specific cooling power must be achieved for AMR heat pumps to become viable. For any given MCM and maximum magnetic field, increasing the specific cooling power necessitates a higher frequency of magnetization and demagnetization, and in turn, a higher frequency of HTF flow. Therefore, for effective heat transfer, an HTF with high thermal conductivity is preferred [13] to increase the rate of heat transfer between the MCM and the HTF. Liquid metals are especially suitable to this application due to them exhibiting orders of magnitude higher thermal conductivity than conventional liquid HTFs. Examples of liquid metal HTFs include lead [14], sodium [14,15], gallium [16], (Sn-50Bi-2Zn)-7Ga [17], and GaInSn (Galinstan) [18–22]. Of these, Galinstan is attractive due to its nontoxicity, desirable thermal conductivity, and relatively small kinematic viscosity [21]. Furthermore, Galinstan has a high surface tension (~0.72 N/m), making it unaffected by the presence of small cracks or imperfect seals when subjected to moderate pressure [23].

Although the potential performance of magnetocaloric refrigeration is high, the working fluid and MCMs are still an active area of research. Thus, the purpose of this paper is to study the compatibility of Galinstan with MCMs and the typical components used for moving fluids in AMR systems. This paper reports on the procedures and the results of the material characterization to determine the compatibility of Galinstan and La-Fe-Si-Mn-H MCM. The study aim was not to identify the mechanism of the interaction between the two components, but rather to verify the composition of the materials. X-ray diffraction (XRD) and X-ray fluorescence (XRF) were performed to identify the phases and the chemicals in the two components. From this investigation it was found that Galinstan will likely have compatibility issues in systems with common components.

2. Materials and Methods

2.1. AMR Experiments

Galinstan is the commercial name for a eutectic gallium–tin–indium alloy (66.0% Ga, 20.5% In, and 13.5% Sn by weight [23]) that is in liquid state at room temperature. Galinstan was chosen for these experiments because it has desirable heat transfer properties such as thermal conductivity (k), thermal diffusivity (α), density (ρ), and specific heat (c_p). The typical properties of Galinstan are k = 16.5 [W/m-K], ρ = 6440 [kg/m^3], and c_p = 296 [J/kg-K] (at 20 °C) [23], resulting in a thermal diffusivity of $\alpha = 8.7 \times 10^{-6}$ [m^2/s], which is an order of magnitude higher than water.

Heat transfer oils are also commonly used as heat transfer fluids but their conductivity is much lower, resulting in smaller thermal diffusivities. The use of Galinstan as an HTF in an AMR that uses La-Fe-Si-Mn-H MCM was attempted due to the beneficial heat transfer properties [4]. The AMR device consisted of a Halbach array (see Figure 1), which contained La-Fe-Si-Mn-H MCM (see Section 2.2 for sample details). It was designed to produce a uniform magnetic field ranging from less than 0.04 T to 1.5 T, which spanned 12 inches along the centerline of the array. The prototype was initially run at 2 Hz, in which a hot-end heat sink temperature of 35 °C and cold-end sink temperature of 27 °C were observed. Before adding Galinstan to the system, magnetic field measurements were performed at distances of 0, 1.94, 4.21, and 6.44 inches from the middle point of the array for different rotating angles. A reference angle of 0°, which represents the minimum field angle, corresponds to the freely resting position of the array. After the magnetic field measurements, Galinstan was added to the system. Here, high-pressure hydraulic cylinders driven by linear actuators

were used to pump the Galinstan through the regenerator, which was surrounded by a series of magnets to form the array.

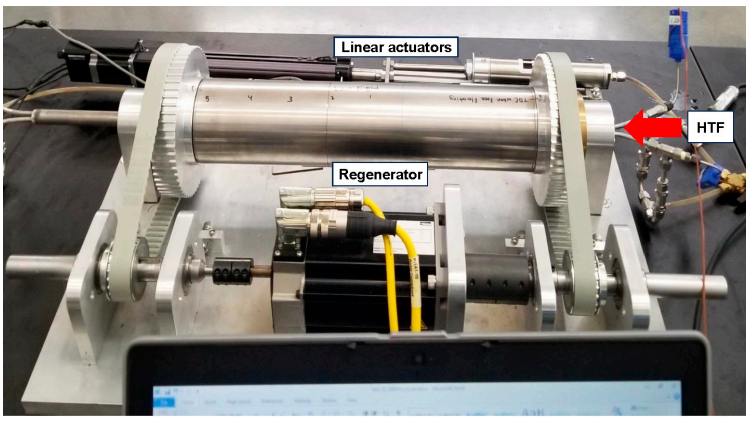

Figure 1. AMR device consisting of a Halbach array and an HTF passing through the array, in combination with linear actuators.

2.2. La-Fe-Si-Mn-H MCM Powder Preparation

MCM powders with a composition of $LaFe_{13-x-y}Mn_xSi_yH_{1.6}$ (x = 0.23–0.34, y = 1.23–1.30), labeled S1–S11, were obtained from Vacuumschmelze. These samples were chosen due to their potential as a working material for room-temperature magnetic refrigeration [9]. The addition of hydrogen increases the Curie temperature (T_c) of the powder to room temperature, while adding Mn allows for the fine-tuning of T_c [2,4]. These powders had T_c values ranging from 19.7 to 41.0 °C (see Table 1) and were used in the AMR regenerator. The as-received MCM powders were used as the baseline for comparison. Some powders were exposed to Galinstan (denoted as samples $S1_{mix}$–$S11_{mix}$) in an AMR experiment where Galinstan was the heat transfer fluid, as shown in Figure 1. For this experiment, the powders were placed in order from S1 to S11 inside the Halbach array.

Table 1. Composition and Curie temperature for the magnetocaloric powders S1–S11.

Powder	Composition	Curie Temperature (°C)
S1	$LaFe_{11.37}Mn_{0.34}Si_{1.29}H_{1.6}$	19.7
S2	$LaFe_{11.38}Mn_{0.32}Si_{1.30}H_{1.6}$	22.2
S3	$LaFe_{11.42}Mn_{0.32}Si_{1.27}H_{1.6}$	23.6
S4	$LaFe_{11.44}Mn_{0.31}Si_{1.25}H_{1.6}$	26.9
S5	$LaFe_{11.40}Mn_{0.31}Si_{1.29}H_{1.6}$	28.3
S6	$LaFe_{11.47}Mn_{0.29}Si_{1.24}H_{1.6}$	30.5
S7	$LaFe_{11.48}Mn_{0.27}Si_{1.24}H_{1.6}$	32.0
S8	$LaFe_{11.47}Mn_{0.27}Si_{1.27}H_{1.6}$	33.5
S9	$LaFe_{11.50}Mn_{0.24}Si_{1.26}H_{1.6}$	36.3
S10	$LaFe_{11.50}Mn_{0.22}Si_{1.27}H_{1.6}$	37.7
S11	$LaFe_{11.54}Mn_{0.23}Si_{1.23}H_{1.6}$	41.0

2.3. X-ray Diffraction and Fluorescence

The XRD characterization was performed at the Institute for Advanced Materials & Manufacturing (IAMM) Diffraction Facility located at the University of Tennessee using a PANalytical Empyrean diffractometer. The X-ray consisted of a Co beam with a K-alpha wavelength of 1.79 Å, and the diffraction angle 2θ ranged between 10 and 100 degrees. To analyze the crystal phases in the powder, phase identification and quantitative phase analysis were performed via the GSAS-II software (version 5715) [24] in combination with Highscore Plus using the Powder Diffraction File-4+ (PDF-4+) database [25]. An additional qualitative analysis using XRF was performed to analyze the chemical composition of the MCM powder. The characterization was conducted using an Epsilon 1 from Malvern

Panalytical via a Ag anode with a maximum voltage of 50 kV and maximum current of 0.5 mA. This instrument allows for the identification of elements ranging from F to Am.

3. Results and Discussion

It was also found that the prototype exhibited a cooling capacity of 34 watts for a COP of 0.4. Figure 2 shows the results of the preliminary magnetic field measurements that were performed at distances of 0, 1.94, 4.21, and 6.44 inches from the middle point of the array for rotating angles of 0–~200°. It was found that magnetic field strength exhibited a generally increasing trend with respect to the rotation angle, wherein it increased from ~0.4 T to 1.3 T. Furthermore, the curve had a characteristically sigmoidal shape, in which the field strength appeared to saturate at angles greater than 150°. Lastly, the similarity in the curves indicated the presence of a uniform magnetic field during the experiment.

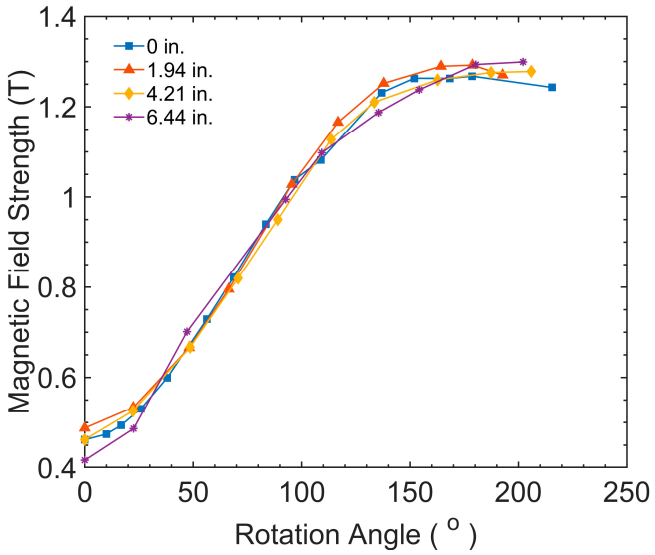

Figure 2. Magnetic field strength vs. rotation angle data for distances of 0, 1.94 in., 4.21 in., and 6.44 from the middle point of the Halbach array.

Once the Galinstan was added, the pressure of the system began to continuously increase, even when the system was at rest. Over a period of one week, the pressure and the temperature of the system increased by ~207 kPa (30 psi) and 5 °C, respectively. Furthermore, a rather large hole was present in the MCM material in a section of the tube that was cut out of the AMR system. It was suspected that the hole and the increases in the system pressure and temperature were due to reactions between the Galinstan and the MCM. To test this hypothesis, material characterization was performed on the MCM before and after exposure to the Galinstan.

Figure 3a,b display the normalized intensity vs. scattering angle for the as-received and Galinstan-exposed samples. The numerous peaks throughout the diffraction pattern indicate that the samples had a highly crystalline structure. Comparison of the patterns from both figures showed no significant difference in the peak widths, suggesting that exposure to Galinstan during the experiment did not change the crystallite size in the powder. Figure 3a features the results for the as-received powders S1–S11, where the three largest peaks were centered at angles of 40.4°, 44.5°, and 54.3°. From these results, no significant differences between the patterns were observed. Figure 3b shows the XRD patterns for the Galinstan-containing powders $S1_{mix}$–$S11_{mix}$. It was found that although the patterns were quite similar to the ones for the as-received samples, there were some key differences. As can be seen in Figure 3b, there were some additional peaks in the patterns (marked by black lines) that were not detected in the as-received powders. For samples $S1_{mix}$–$S11_{mix}$, a shoulder peak was observed at a scattering angle of ~24.9° and additional peaks were observed at angles of 39.4°, 41.3° (except sample $S8_{mix}$), and 43.5°. For samples

$S9_{mix}$–$S11_{mix}$, some additional peaks were found. These peaks were centered at 29.5° and 49°, while another peak was detected in sample $S11_{mix}$ at an angle of 38.5°. It was thought that these peaks may have been the result of chemical reactions and impurities during the AMR experiment.

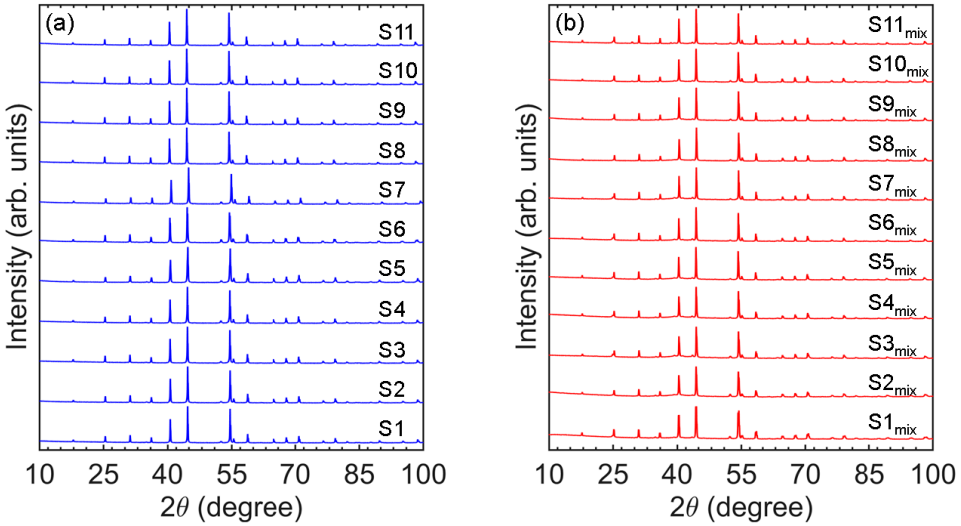

Figure 3. The XRD patterns for the (**a**) as-received (samples S1–S11) and (**b**) Galinstan-exposed (samples $S1_{mix}$–$S11_{mix}$) MCMs. Black lines denote the peaks not observed in the as-received powders.

Figure 4 shows the diffraction pattern collected for S5. The inset reveals a peak on the left shoulder of each characteristic LaFeSiH peak. It should be noted that this additional peak appears for all LaFeSiH peaks, not just the three represented in the inset. The existence of these shoulder peaks is indicative of a second LaFeSiH phase with the same crystallographic space group but a slightly different lattice parameter, which was likely caused by a small difference in stoichiometry.

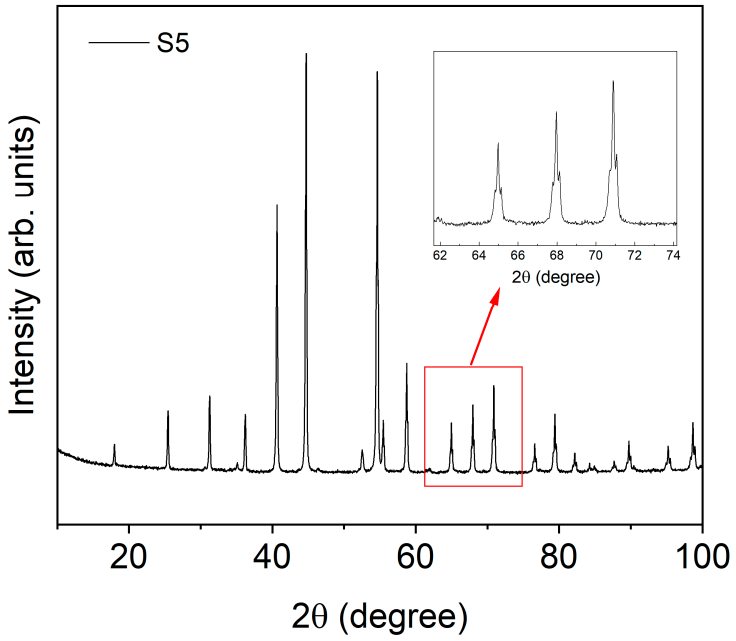

Figure 4. The XRD pattern for sample S5. The inset features three primary peaks with shoulder peaks on them that represent the second LaFeSiH phase.

The results of subsequent XRF characterization of the Galinstan-exposed powder $S11_{mix}$ can be seen in Figure 5. The spectra consisted of five prominent peaks that were

centered at energies of approximately 25.2 keV, 26.3 keV, 27.3 keV, 28.5 keV, and 29.7 keV. These results revealed that the powder contained Sn, In, and Sb (marked by a red box in the figure), although the exact amounts could not be determined due the qualitative nature of the XRF measurement. Of the detected elements, Sb was the only one that was not expected to be present and was therefore likely an impurity in the sample. This result indicates that the anomalous peaks observed in the XRD patterns for samples $S9_{mix}$–$S11_{mix}$ from Figure 3b likely corresponded to the presence of Sb in the powder.

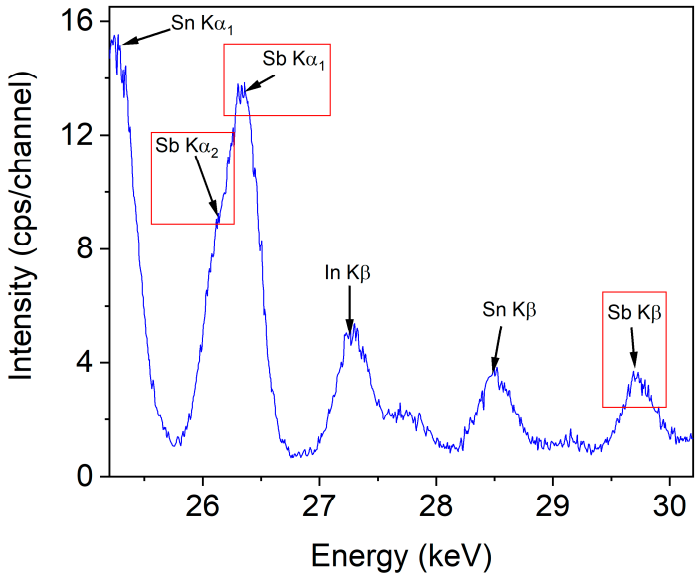

Figure 5. The results of the XRF analysis of the Galinstan-exposed magnetocaloric powder $S11_{mix}$. The red boxes denote the peaks that were associated with the Sb in the powder.

The results of the Rietveld refinement phase ID analysis for the as-received and Galinstan-exposed MCMs are presented in Table 2, Tables S1 and S2 (Supplementary Materials). Both the as-received and Galinstan-exposed powders were found to contain the cubic phases $LaFe_{11.31}Si_{1.61}H_{1.51}$ (space group $Fm\bar{3}c$ (226)) and Mn_3Si (space group $Fm\bar{3}m$ (225)), as well as a hexagonal phase La_2O_3 (space group $P\bar{3}m1$ (164)). The Galinstan-exposed powders were also found to consist of Ga- and Sb-containing phases, which were likely responsible for the additional peaks observed in Figure 3b. These phases consisted of the orthorhombic phase GaO(OH) (space group Pnma (62)), cubic phase GaSb (space group $F\bar{4}3m$ (216)), and tetragonal phase $LaMn_{0.87}Sb_2$ (space group P4/nmm (129)). However, it should be mentioned that the GaSb phase was only observed in samples $S9_{mix}$–$S11_{mix}$, while the $LaMn_{0.87}Sb_2$ phase was only found in sample $S11_{mix}$.

Table 2. Results of the phase quantification analysis (wt. %) for the as-received (top) (samples S1–S11) and Galinstan-containing (bottom) MCM powders (samples $S1_{mix}$–$S11_{mix}$). The LaFeSiH phase has been designated as I and II to represent that there exist two phases with the same space group but slightly different lattice parameters, indicating that the two phases have slightly different stoichiometries.

Powder	$LaFe_{11.31}Si_{1.61}H_{1.51}$ I	$LaFe_{11.31}Si_{1.61}H_{1.51}$ II	GaO(OH)	La_2O_3	Mn_3Si	GaSb	$LaMn_{0.87}Sb_2$
S1	8.1	88.2	0	0.5	3.1	0	0
S2	22.5	74.1	0	0.6	2.8	0	0
S3	23.0	73.5	0	0.4	3.1	0	0
S4	31.9	63.5	0	0.4	4.2	0	0
S5	54.7	42.3	0	0.4	2.5	0	0
S6	63.2	31.8	0	0.4	4.6	0	0
S7	93.2	1.5	0	0.8	4.5	0	0
S8	93.8	1.3	0	0.5	4.4	0	0
S9	94.3	0.9	0	0.5	4.3	0	0
S10	93.3	1.2	0	0.6	4.9	0	0
S11	93.9	0.2	0	0.4	5.5	0	0

Table 2. *Cont.*

Powder	$LaFe_{11.31}Si_{1.61}H_{1.51}$ I	$LaFe_{11.31}Si_{1.61}H_{1.51}$ II	GaO(OH)	La_2O_3	Mn_3Si	GaSb	$LaMn_{0.87}Sb_2$
$S1_{mix}$	55.7	36.7	4.4	0.6	2.6	0	0
$S2_{mix}$	78.9	14.3	2.4	0.8	3.5	0	0
$S3_{mix}$	75	12.2	9.3	0.4	3.1	0	0
$S4_{mix}$	79.3	11	7.3	0.5	1.9	0	0
$S5_{mix}$	90.9	0.3	6.3	0.5	2.0	0	0
$S6_{mix}$	87.2	0.2	10.3	0.5	1.8	0	0
$S7_{mix}$	86.5	1.9	9.1	0.5	2.0	0	0
$S8_{mix}$	94.8	0	2.2	0.5	2.4	0	0
$S9_{mix}$	92.1	0	4.4	0.5	2.7	0.3	0
$S10_{mix}$	92.5	0	4.1	0.5	2.5	0.3	0
$S11_{mix}$	87.3	0	8.3	0.4	2.5	0.9	0.6

Figure 6a,b provide a more detailed comparison of sample S11 before and after Galinstan exposure ($S11_{mix}$). Similar to Figure 3, XRD patterns are displayed for the scattering angles of 10–100° and the peaks are indexed according to their different phases. These powders were chosen since the $S11_{mix}$ powder contained the largest number of different phases, suggesting that it underwent the greatest degree of chemical reaction during the AMR experiment. Both the as-received and Galinstan-exposed powders were found to contain the cubic phases $LaFe_{11.31}Si_{1.61}H_{1.51}$ (space group $Fm\bar{3}c$ (226)) and Mn_3Si (space group $Fm\bar{3}m$ (225)), as well as a hexagonal phase La_2O_3 (space group $P\bar{3}m1$ (164)). The Galinstan-exposed powders were also found to consist of the orthorhombic phase GaO(OH) (space group Pnma (62)), cubic phase GaSb (space group $F\bar{4}3m$ (216)), and tetragonal phase $LaMn_{0.87}Sb_2$ (space group P4/nmm (129)). The results further confirm that these impurity phases were responsible for the additional peaks observed in Figure 3b.

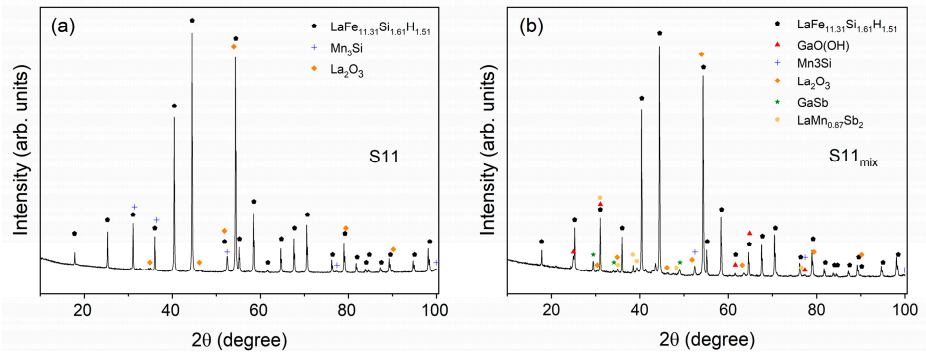

Figure 6. The indexed XRD patterns for the (**a**) as-received (sample S11) and (**b**) Galinstan-exposed (sample $S11_{mix}$) MCMs.

A more in-depth quantitative analysis of the powders (see Tables S1 and S2 from the Supplementary Materials) revealed the following. It was found that the magnetocaloric $LaFe_{11.31}Si_{1.61}H_{1.51}$ phase comprised >94 wt.% of the as-received powder. Furthermore, there were two types of this phase (labelled $LaFe_{11.31}Si_{1.61}H_{1.51}$ I and $LaFe_{11.31}Si_{1.61}H_{1.51}$ II) with slightly different unit cell volumes (determined by the Rietveld refinement). For the as-received powder, this difference exhibited a generally increasing trend with respect to the sample number, in which the maximum difference was found to be ~41 $Å^3$ (sample S11). The two different unit cell volumes may have been the result of slight stoichiometric differences. Further comparison of the two magnetocaloric phases found that the $LaFe_{11.31}Si_{1.61}H_{1.51}$ I phase underwent a greater change in its unit cell volume after exposure to Galinstan when compared to the second phase. For the former, the change in cell volume ranged from ~1 $Å^3$ to ~40 $Å^3$ (samples S7 and $S7_{mix}$), while a maximum change of ~16 $Å^3$ occurred in the latter. The GaO(OH) phase that was detected in the Galinstan-exposed powders had an average unit cell volume of ~134.00 $Å^3$. With respect to the Mn_3Si and La_2O_3 phases, they exhibited a change of less than <1 $Å^3$ after exposure. In terms of the GaSb and $LaMn_{0.87}Sb_2$ phases observed in powders $S9_{mix}$–$S11_{mix}$, they had unit cell volumes of 228.10 $Å^3$ and 212.89 $Å^3$, respectively. It was also found that expo-

sure to Galinstan led to an average reduction of 4.87 wt.% of the original magnetocaloric $LaFe_{11.31}Si_{1.61}H_{1.51}$ phases. Lastly, in the as-received powder, there was also a general increase in the amount of Mn_3Sn phase present with respect to the sample number. For more detail on the results of the Rietveld refinement, please see Tables S1 and S2.

As discussed previously, Sb-containing phases GaSb and $LaMn_{0.87}Sb_2$ were found in samples $S9_{mix}$–$S11_{mix}$, which was near the degraded MCM matrix regions in the tube. Furthermore, the $LaFe_{11.31}Si_{1.61}H_{1.51}$ II phase was not observed in samples $S8_{mix}$–$S11_{mix}$, although the reason for there only being one of the MCM phases in these mixtures is not well understood. The presence of Sb in the powder may be due to trace amounts of Sb in the Galinstan or contamination due to components in the system. The contamination may have resulted from corrosion of the array materials due to Galinstan exposure [23]. The Sb and Ga in the liquid eutectic formed solid GaSb, while the Sb reacted with La and Mn in the MCM matrix to form the $LaMn_{0.87}Sb_2$ compound.

The reduction in the magnetocaloric phase was accompanied by the emergence of a GaO(OH) phase. The amount of this phase ranged from 2.2 to 10.3 wt.%. It is interesting to note that the maximum amount of this phase was observed in sample $S6_{mix}$, which was located in the middle of the regenerator tube. This phase may have resulted from a release of H from the powder, which then reacts with oxygen in the environment. Subsequently, the GaO(OH) compound may have formed via an exothermic reaction (−705.3 kJ/mol [26]) of Ga with the OH anions and O_2 in the environment via the following chemical equation [27]:

$$2Ga_{(l)} + 2OH^-_{(aq)} + O_{2(aq)} \rightarrow 2GaO(OH)_s \quad \Delta H^o = -705.3\ kJ/mol \tag{1}$$

This exothermic reaction, therefore, may have been the reason for the observed temperature and pressure increases during the AMR experiment. However, future work will be needed to confirm this hypothesis.

The results, as presented above, provide strong evidence that the pressure and temperature increases observed during the AMR experiment were the result of chemical reactions between the liquid Galinstan and the MCM. Additionally, these reactions indicate that the MCM was not compatible with Galinstan. Despite this issue, there may be other potential MCM candidates for this AMR application such as Gd, due to its resistance to Galinstan [18].

4. Conclusions

For this work, the effects of liquid Galinstan exposure on the phase stability of $LaFe_{13-x-y}Mn_xSi_yH_{1.6}$ magnetocaloric powders in an AMR system were investigated. Preliminary tests showed that during the experiment, the system exhibited a uniform magnetic field that coincided with a pressure and temperature increase. The powders were characterized using XRD and XRF methods, and the phases were determined using software in combination with the Rietveld refinement technique. For the as-received powder, some oxygen-containing phases were present, while for the Galinstan-exposed MCM powder, gallium-, antimony-, oxygen-, and hydroxide-containing phases were observed. The antimony-containing phases were likely due to trace amounts of antimony being present in the Galinstan during the experiment. An exothermic reaction, which may have resulted from a reaction between the liquid Ga and OH^- ion, was identified as the source of the measured pressure and temperature increases (Equation (1)) in the AMR system. The results of this study indicated that the MCM powders tested are not compatible with liquid Galinstan in the presence of aqueous hydroxide and oxygen (both found in water), suggesting further studies should be conducted in moisture-free environments.

Supplementary Materials: The following supporting information can be downloaded at https://www.mdpi.com/article/10.3390/magnetochemistry10020013/s1: Table S1: Results of the qualitative and quantitative phase analyses for the as-received powders S1–S11; Table S2: Results of the qualitative and quantitative phase analyses for the Galinstan-exposed powders $S1_{mix}$–$S11_{mix}$.

Author Contributions: Conceptualization, J.R., K.N. and A.M.M.; methodology, J.B., M.Z. and M.R.K.; validation, J.B. and J.R.; formal analysis, J.B., J.R. and M.R.K.; investigation, J.B. and J.R., M.Z. and M.R.K.; resources, M.Z., K.N. and A.M.M.; data curation, J.B. and M.R.K.; writing—original draft preparation, J.B. and J.R.; writing—review and editing, J.B., J.R., M.Z., M.R.K., K.N. and A.M.M.; visualization, J.B.; supervision, A.M.M.; project administration, A.M.M.; funding acquisition, A.M.M. All authors have read and agreed to the published version of the manuscript.

Funding: This material is based upon work supported by the U.S. Department of Energy, Building Technologies Office under contract DE-AC05-00OR22725.

Data Availability Statement: The data presented in this study are available on request from the corresponding author. The data are not publicly available due to privacy/ethical reasons.

Acknowledgments: This research used resources of the Oak Ridge Leadership Building Technologies Research and Integration (BTRIC) Facility, which is a DOE Office of Science User Facility. The X-ray diffraction (XRD) characterization was performed at the Institute for Advanced Materials & Manufacturing (IAMM) Diffraction Facility located at the University of Tennessee. Lastly, the authors would like to thank Vacuumschmelze for providing the MCM powders.

Conflicts of Interest: The authors declare no conflicts of interest.

References

1. Koshkid'ko, Y.S.; Dilmieva, E.T.; Cwik, J.; Rogacki, K.; Kowalska, D.; Kamantsev, A.P.; Koledov, V.V.; Mashirov, A.V.; Shavrov, V.G.; Valkov, V.I.; et al. Giant reversible adiabatic temperature change and isothermal heat transfer of MnAs single crystals studied by direct method in high magnetic fields. *J. Alloys Compd.* **2019**, *798*, 810–819. [CrossRef]
2. Zhang, M.K.; Abdelaziz, O.; Momen, A.M.; Abu-Heiba, A. A numerical analysis of a magnetocaloric refrigerator with a 16-layer regenerator. *Sci. Rep.* **2017**, *7*, 12. [CrossRef] [PubMed]
3. Pecharsky, V.K.; Gschneidner, K.A. Giant magnetocaloric effect in $Gd_5(Si_2Ge_2)$. *Phys. Rev. Lett.* **1997**, *78*, 4494–4497. [CrossRef]
4. Barcza, A.; Katter, M.; Zellmann, V.; Russek, S.; Jacobs, S.; Zimm, C. Stability and Magnetocaloric Properties of Sintered La(Fe, Mn, Si)$_{13}H_z$ Alloys. *IEEE Trans. Magn.* **2011**, *47*, 3391–3394. [CrossRef]
5. Hu, F.X.; Shen, B.G.; Sun, J.R.; Wang, G.J.; Cheng, Z.H. Very large magnetic entropy change near room temperature in $LaFe_{11.2}Co_{0.7}Si_{1.1}$. *Appl. Phys. Lett.* **2002**, *80*, 826–828. [CrossRef]
6. Fujita, A.; Fujieda, S.; Hasegawa, Y.; Fukamichi, K. Itinerant-electron metamagnetic transition and large magnetocaloric effects in $La(Fe_xSi_{1-x})_{13}$ compounds and their hydrides. *Phys. Rev. B* **2003**, *67*, 104416. [CrossRef]
7. Wada, H.; Tanabe, Y. Giant magnetocaloric effect of $MnAs_{1-x}Sb_x$. *Appl. Phys. Lett.* **2001**, *79*, 3302–3304. [CrossRef]
8. Tegus, O.; Brück, E.; Buschow, K.H.J.; de Boer, F.R. Transition-metal-based magnetic refrigerants for room-temperature applications. *Nature* **2002**, *415*, 150–152. [CrossRef]
9. Katter, M.; Zellmann, V.; Reppel, G.W.; Uestuener, K. Magnetocaloric Properties of La(Fe, Co, Si)$_{13}$ Bulk Material Prepared by Powder Metallurgy. *IEEE Trans. Magn.* **2008**, *44*, 3044–3047. [CrossRef]
10. Barclay, J.A.; Steyert, W.A. Active Magnetic Regenerator. US Patent 4,332,135, 6 January 1982.
11. Gomez, J.R.; Garcia, R.F.; Catoira, A.D.; Gomez, M.R. Magnetocaloric effect: A review of the thermodynamic cycles in magnetic refrigeration. *Renew. Sustain. Energ. Rev.* **2013**, *17*, 74–82. [CrossRef]
12. Kamran, M.S.; Ahmad, H.O.; Wang, H.S. Review on the developments of active magnetic regenerator refrigerators—Evaluated by performance. *Renew. Sustain. Energ. Rev.* **2020**, *133*, 16. [CrossRef]
13. Manservisi, S.; Menghini, F. A CFD four parameter heat transfer turbulence model for engineering applications in heavy liquid metals. *Int. J. Heat Mass Transf.* **2014**, *69*, 312–326. [CrossRef]
14. Niedermeier, K. A perspective on high-temperature heat storage using liquid metal as heat transfer fluid. *Energy Storage* **2023**, *5*, e530. [CrossRef]
15. Sarvghad, M.; Ong, T.C.; Bell, S.; Rumman, R.; Maher, S.D.; Woodcock, J.W.; Will, G.; Andersson, G.; Lewis, D.A.; Steinberg, T.A. On the compatibility of liquid sodium as heat transfer fluid for advanced concentrated solar thermal energy systems. *Sol. Energy Mater. Sol. Cells* **2022**, *246*, 111897. [CrossRef]
16. Liu, G.L.; Liu, J. Convective Cooling of Compact Electronic Devices Via Liquid Metals with Low Melting Points. *J. Heat Transf.-Trans. Asme* **2021**, *143*, 050801. [CrossRef]
17. Wang, Q.M.; Cheng, X.M.; Li, Y.Y.; Yu, G.M.; Liu, Z. High-temperature corrosion of Sn-Bi-Zn-Ga alloys as heat transfer fluid. *Rare Met.* **2021**, *40*, 2221–2229. [CrossRef]

18. Scarpa, F.; Slimani, S. Galinstan liquid metal as the heat transfer fluid in magnetic refrigeration. *Appl. Therm. Eng.* **2023**, *232*, 120971. [CrossRef]
19. Zhang, Z.K.; Lei, J.M.; Li, F.J.; Li, L.; Li, S.M.; Huang, Y.B.; Feng, K.; Tan, Q.; Lu, X.L. Investigation of the heat transfer characteristics of Galinstan liquid metal driven by electromagnetism. *Appl. Therm. Eng.* **2023**, *230*, 120776. [CrossRef]
20. Wang, C.T.; Lu, Q.; Liu, Y.; Huang, H.J.; Sun, J. Progressive review of heat transfer enhancement technologies in 2010–2020. *Sustain. Energy Technol. Assess.* **2023**, *56*, 103121. [CrossRef]
21. Zhang, X.D.; Yang, X.H.; Zhou, Y.X.; Rao, W.; Gao, J.Y.; Ding, Y.J.; Shu, Q.Q.; Liu, J. Experimental investigation of galinstan based minichannel cooling for high heat flux and large heat power thermal management. *Energy Convers. Manag.* **2019**, *185*, 248–258. [CrossRef]
22. Zhang, R.; Hodes, M.; Lower, N.; Wilcoxon, R. Water-Based Microchannel and Galinstan-Based Minichannel Cooling beyond 1 kW/cm^2 Heat Flux. *IEEE Trans. Compon. Packag. Manuf. Technol.* **2015**, *5*, 762–770. [CrossRef]
23. Hodes, M.; Zhang, R.; Lam, L.S.; Wilcoxon, R.; Lower, N. On the Potential of Galinstan-Based Minichannel and Minigap Cooling. *IEEE Trans. Compon. Packag. Manuf. Technol.* **2014**, *4*, 46–56. [CrossRef]
24. Toby, B.H. EXPGUI, a graphical user interface for GSAS. *J. Appl. Crystallogr.* **2001**, *34*, 210–213. [CrossRef]
25. Gates-Rector, S.; Blanton, T. The Powder Diffraction File: A quality materials characterization database. *Powder Diffr.* **2019**, *34*, 352–360. [CrossRef]
26. Pokrovski, G.S.; Diakonov, I.I.; Benezeth, P.; Gurevich, V.M.; Gavrichev, K.S.; Gorbunov, V.E.; Dandurand, J.L.; Schott, J.; Khodakovsky, I.L. Thermodynamic properties of gallium hydroxide oxide (alpha-GaOOH) at temperatures to 700 K. *Eur. J. Mineral.* **1997**, *9*, 941–951. [CrossRef]
27. Kumar, V.B.; Gedanken, A.; Porat, Z.e. Facile synthesis of gallium oxide hydroxide by ultrasonic irradiation of molten gallium in water. *Ultrason. Sonochem.* **2015**, *26*, 340–344. [CrossRef] [PubMed]